Comparative Evaluation of Modulation Strategies for a Single-Phase PV Micro-Inverter with High-Frequency Transformer

Jonatas Rodrigo Kinas, Diego A. Acevedo-Bueno, Gabriel Sales Lins Rodrigues, Montiê Alves Vitorino, Alexandre Cunha Oliveira and Antônio Marcus Nogueira Lima
Department of Electrical Engineering
Federal University of Campina Grande (UFCG) – Campina Grande, PB, Brazil
Email: [jonatas.kinas; diego.bueno; gabriel.rodrigues]@ee.ufcg.edu.br, [vitorino; aco; amnlima]@dee.ufcg.edu.br

***Abstract*—Micro-inverter topologies have several advantages for grid-connected photovoltaic (PV) power generation systems, such as: flexible system design, simplified installation and enhanced safety characteristics. In this paper, a single-phase micro-inverter with a high-frequency transformer is introduced. The micro-inverter is composed by: an isolated high-frequency full bridge dc-dc converter, an inverter and LCL filter. Performance evaluation of the converter using three modulation strategies are analyzed by comparing harmonic distortion of injected current and semiconductor losses. The aforementioned modulation strategies (MS) are: phase-shift with unipolar PWM (MS1), phase-shift with hybrid PWM (MS2), and sinusoidal phase-shift with unfolding stage (MS3). Simulation results using PSIM corroborate the feasibility of the micro-inverter adopting different modulation strategies, being MS2 more equilibrated between semiconductor losses and injected current THD. Finally, a 250 W prototype was manufactured to validate the performance of the micro-inverter.**

I. Introduction

The demand for electricity has been growing at rate of 2.3% since the beginning of century [1]. As response to this increase and new environmental commitments on greenhouse gas emissions, the insertion of renewable sources into the grid has been intensified. Among these sources, photovoltaic (PV) systems represent a convenient alternative for improving the availability factor of the power system.

Depending on the nominal power of PV installation, different configurations has been presented in the literature. For residential applications, string and ac module configurations are preferred, offering well differentiated characteristics [2], [3]. On the one hand, string configuration is composed by series connected panel set and a single DC-AC inverter and is preferred by cost considerations. However, this configuration presents some limitations such as: high-voltage DC cables required, mismatch losses, low MPPT efficiency (centralized scheme) and reduced flexibility [4]. On the other hand, ac module configuration is composed by a single PV panel and a micro-inverter connected directly to the grid by a plug-and-play system [3], [5]. In contrast, ac module allows: flexible design, simplified installation, high efficiency MPPT and enhanced safety characteristics.

Typically, the input voltage of the micro-inverter is in the range of 15 to 40 V, so high voltage gain is required for grid connection. To attain this, topologies without and with galvanic isolation have been proposed as summarized in [6]–[8]. Among the former, there are purposes based on boost converters as the following: a single-stage coupled-inductor double-boost inverter with synchronized PWM strategy [9]; and a two-stage system with high gain ZVS-interleaved boost converter [10]. Also, topologies with impedance network and controlled shoot-through state are also competitive solutions for non-isolated grid-connected applications [11], [12]. Due to safety considerations, latter topologies with high-frequency (HF) transformers are preferred for this applications.

Single-stage isolated topologies based on flyback converter furnish low price, low semiconductor devices count and non complex control. Nevertheless, high current stress on switches and high losses reduce effective operational area and efficiency [13]. Also, forward-type micro-inverter topologies are available, but they demonstrated poor THD performance and more complex transformer design [14]. Besides, topologies formed by HF full-bridge (FB) and cycloconverter could be considered as single-stage and they feature higher efficiency even with elevated number of devices. The disadvantage of these topologies lies in complexity and cost increase [15], [16]. A comparative study of three topologies with cycloconverter at the output clarified that HF half-bridge yields comparable efficiency with lower losses than HF FB and HF push-pull converters [17].

Two-stage PV micro-inverter topologies are composed by an isolated dc-dc converter and an unfolding/PWM inverter. In [18], [19], an isolated boost half-bridge dc-dc first stage handles MPPT and voltage boosting whilst achieving ZVS in the two active switches by proper HF transformer design. A plug-in repetitive controller is responsible for injecting low THD current under wide load conditions in the grid side. In [20], an evaluation of five two-stage topologies with pulsed dc-link and unfolding stage was carried out and a dual-LCL series resonant sinusoidally modulated inverter proved to have higher efficiency and ZVS in all devices. The remain tested topologies were: a variable-frequency PWM converter and

978-1-5386-1180-7/18/$31.00 ©2018 IEEE

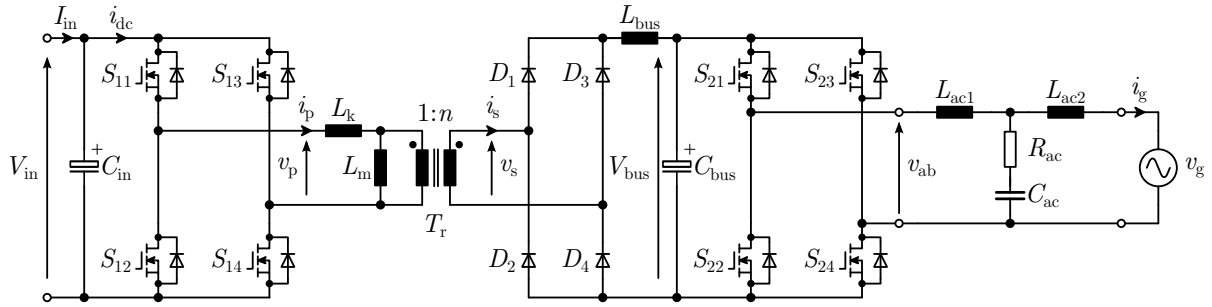

Fig. 1. Power converter topology. Input side HF Full-bridge DC-AC, HF transformer, rectifier bridge, LC dc-link filter, output side PWM inverter and LCL filter.

three fixed-frequency series resonant converters (SRC).

This paper introduces a comparative study of three modulation strategies (MS) for a grid-connected two-stage micro-inverter formed by an isolated high-frequency full bridge dc-dc converter, a PWM inverter and LCL filter as shown in Fig. 1. The description of the converter and the modulation strategies are outlined in Section II. The proposed control scheme for the converter is described in Section III. Finally, simulation and experimental results are presented in Section IV and V, respectively.

II. Proposed Micro-inverter and Modulation Strategies

Fig. 1 illustrates the topology of the grid-connected two-stage micro-inverter. Switches $S_{11}-S_{14}$ compose the input side FB inverter, whose output is connected to the HF transformer T_r with magnetizing and leakage inductor, L_m and L_k, respectively. The HF transformer ensures galvanic isolation between the PV module and the grid and also provides the required voltage gain. The secondary winding of the transformer feeds the dc-link filter (L_{bus} and C_{bus}) via the uncontrolled rectifier bridge ($D_1 - D_4$). The output side FB inverter composed by $S_{21} - S_{24}$ is connected to the grid through the LCL filter with resistive damping (L_{ac1}, L_{ac2}, C_{ac} and R_{ac}).

For evaluating the performance of the micro-inverter, three modulation strategies were defined: phase-shift with unipolar PWM (MS1), phase-shift with hybrid PWM (MS2), and sinusoidal phase-shift with unfolding stage (MS3). In MS1 and MS2, a constant dc-link is established and the output side FB inverter generates a three-level output voltage for injecting current into the grid. For MS1, the output side inverter uses unipolar PWM. This inverter operates leg *a* at grid frequency and leg *b* at switching frequency for MS2. In contrast with the previous modulation strategies, MS3 imposes a pulsed dc-link at twice the grid frequency on C_{bus} and the output side FB inverter merely transfers this tension to the LCL filter depending on an synchronized reference. This operation allows to replace $S_{21} - S_{24}$ by thyristors because of cost and robustness [8]. Although, the dc-link waveform differs between MS3 and the others two MS, each leg of the input side FB operates with duty cycle of 0.5 and its output voltage is adjusted by the proper phase shift between the leg carriers.

A. LCL filter design considerations

A LCL filter with resistive damping was selected as interface between the micro-inverter and the grid. This kind of filter guarantees an attenuation of $-60\text{dB}/\text{dec}$ for high-order harmonics (above the resonance frequency). The damping resistor connected in series with the capacitor is used for mitigating harmonics close to the resonance frequency. The filter transfer function is given by Eq. (1) (top of the next page) and the resonance frequency by Eq. (2).

$$f_o = \frac{1}{2\pi}\sqrt{\frac{L_{ac1}+L_{ac2}}{L_{ac1}L_{ac2}C_{ac}}} \tag{2}$$

For obtaining an adequate filter design, it is necessary to follow a some considerations. The resonant frequency must be selected into $10f_{ac} \leq f_o \leq f_{sw}/2$. Thereby, inductor L_{ac1} is determined by Eq. (3). In this case, inductor voltage v_{Lac1} is assumed to be 5% of the rated voltage of the grid.

$$L_{ac1} \leq \frac{0,05 v_g \delta}{\Delta i_g f_{sw}} \tag{3}$$

where, Δi_g is the maximum ripple expected in the inverter output current (i_g), δ is the maximum width of the PWM modulation signal and f_{sw} is the switching frequency.

The inductors L_{ac1} and L_{ac2} can be related by the α factor as shown in Eq. (4). According to [21], for obtaining the smallest capacitance of the filter, the α factor must be unitary.

$$L_{ac1} = \alpha L_{ac2} \tag{4}$$

The filter capacitance C_{ac} can be determined by considering that it will absorb 5% of the nominal power as shown in Eq.(5).

$$C_{ac} \leq \frac{0,05 P_{nom}}{2\pi f_{ac} v_g^2} \tag{5}$$

Finally, the damping resistor (R_{ac}) is usually chosen as one-third of the capacitor reactance at the resonant frequency as determined by Eq. (6).

$$R_{ac} = \frac{1}{3}\frac{1}{2\pi f_{ac} C_{ac}} \tag{6}$$

$$\frac{i_g}{v_{ab}} = \frac{sC_{ac}R_{ac}+1}{s^3L_{ac1}L_{ac2}C_{ac}+s^2(L_{ac1}+L_{ac2})C_{ac}R_{ac}+s(L_{ac1}+L_{ac2})} \tag{1}$$

III. Control scheme

The control scheme for MS1 and MS2 is shown in Fig. 2(a). The dc-link voltage (v_{bus}) is controlled by the PI controller, whose output provides the amplitude reference of the injected grid current ($I_{\text{g,ref}}$). A SOGI PLL was implemented to synchronize the phase of the instantaneous grid current reference ($i_{\text{g,ref}}$) with grid voltage (v_g) [22]. Then, the Proportional+Resonant (PR) controller generates the output side voltage reference ($v_{\text{ab,ref}}$). In MS1 and MS2, the incremental conductance MPPT algorithm carries out of imposing the phase shift to the input side FB legs without considering the output side status.

Fig. 2(b) shows the input power control scheme adopted for MS3 [23]. In this case, the amplitude reference of the injected grid current ($I_{\text{g,ref}}$) is obtained by the voltage controller output and the input power feed-forward. The grid current control has the same structure of the previous scheme, however, the voltage reference now should control the angle (ϕ) between the carriers of the input side FB legs and the block *PolSel*, which determines the polarity of output voltage (v_{ab}).

IV. Simulation Results

The proposed modulation strategies were evaluated on the micro-inverter by using PSIM. The employed parameters are summarized in Table I and the physical model of Kyocera KD260GX solar panel. For estimating the semiconductor losses, the characteristics of real devices were inserted in the Thermal Module of PSIM. The devices selected for the micro-inverter were: Texas Instruments CSD19535KCS MOSFET for $S_{11}-S_{14}$, International Rectifiers HFA08TB60PbF diode for D_1-D_4, and ST Microelectronics STF40N65M2 MOSFET for $S_{21}-S_{24}$.

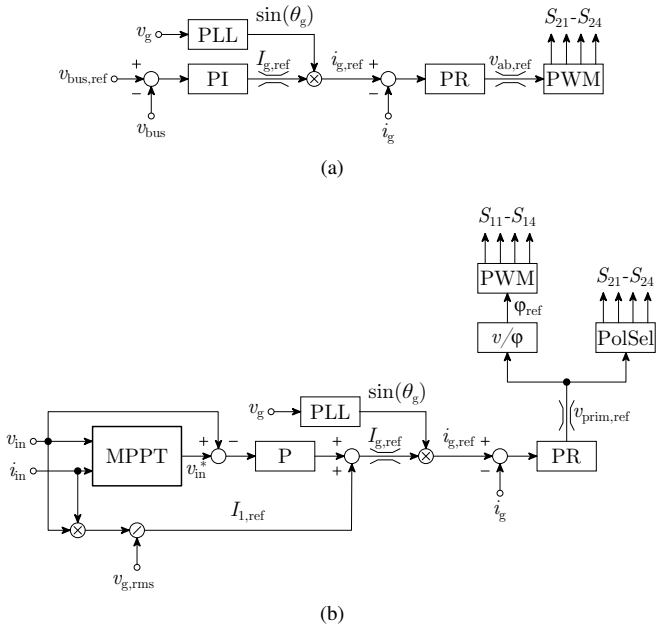

Fig. 2. Control schemes for (a) MS1, MS2 and (b) MS3.

TABLE I
Micro-inverter parameters used in simulation.

Description	Parameter	Value
Nominal output power	P_{nom}	260 W
Input voltage	V_{i}	$30 \sim 40$ V
Grid voltage	v_{g}	220 V_{rms}
Grid frequency	f_{ac}	60 Hz
Switching frequency	f_{sw}	50 kHz
Transformer turns ratio	n	14
Magnetizing inductor	L_{m}	26.8 μH
Leakage inductor	L_{k}	0.2 μH
Input capacitor	C_{in}	470 μF
Dc-link capacitor	C_{bus}	300 μF
Dc-link inductor	L_{bus}	1 mH
Output Filter inductors	L_{ac1}, L_{ac2}	820 μH
Output Filter capacitor	C_{ac}	0.39 μF
Damping resistor	R_{ac}	10.0 Ω

In Fig. 3, simulation results for MS1 are presented. The employed control scheme demonstrated to be able to regulate the dc-link voltage while injecting current into the grid at full load condition as shown in Fig. 3(a). The dynamic response in face of irradiance fluctuations corroborate the correctness of controllers design and the effectiveness of the incremental conductance MPPT as depicted in Fig. 3(b)-(c).

The performance comparison considered following parameters: total losses, total harmonic distortion (THD) and rms value of injected current. Table II shows the simulation results for the three modulation strategies at four different irradiance conditions. As expected, MS1 demonstrated better harmonic performance and higher losses since all the devices in the output FB inverter operate at switching frequency. On other hand, MS2 demonstrated to be more efficient because of unique leg operating at switching frequency.

V. Experimental Results

A 120 W micro-inverter prototype wast build to experimentally validate the modulation strategies as shown in Fig.4. Due to some limitations of power supply system and components (HF transformer), it was not possible to match the simulation and experimental results. Microncontroller TMS320F28379D from Texas Instruments was used for PWM generation altogether with isolated driver Fairchild FOD3180.

Fig. 5 shows the waveforms of output/input voltages and currents in the prototype at nominal power condition. For MS1, the injected current THD is 1.71%, so it complies with

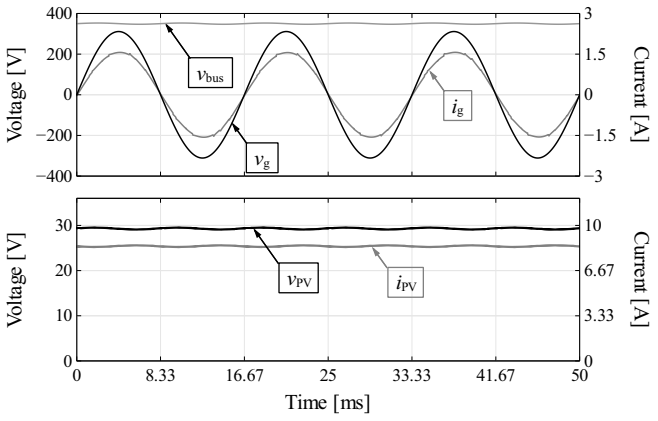

(a)

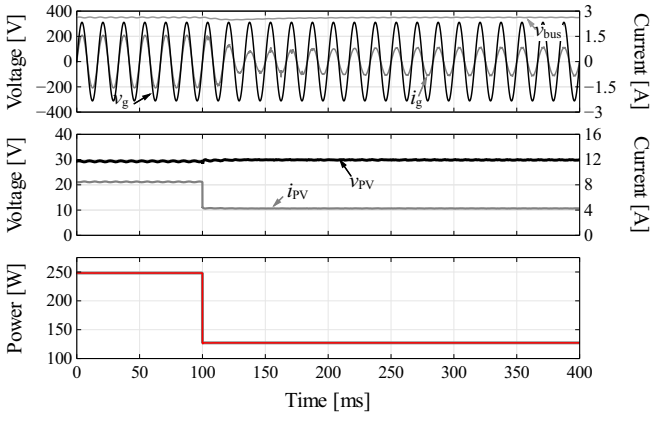

(b)

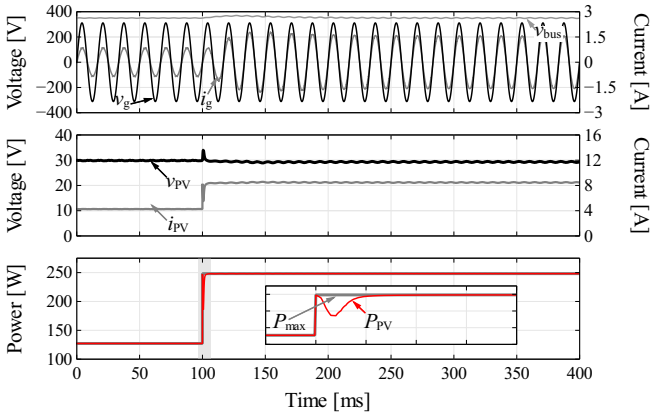

(c)

Fig. 3. Simulation results for modulation strategy 1 (MS1). (a) Input and output voltages and currents. (b) Step-down irradiance transition from 1000 W/m^2 to from 500 W/m^2. (c) Step-up irradiance transition from 500 W/m^2 to from 1000 W/m^2.

the different standards. In the same fashion, MS2 allows to impose an injected current with 2.76% at full load. For MS3, the output current demonstrated zero-crossing error, so current THD arose 4.38%.

In Fig. 6, the main waveforms in the HF transformer are presented. For SM1, the primary current stays the same in the

TABLE II
PERFORMANCE EVALUATION FOR THE PROPOSED MICRO-INVERTER FROM SIMULATION.

E [W/m^2] @ Pmax [W]	**Modulation Strategy**	**Total semicond. Losses [W]**	**THD i_g [%]**	**$i_{g,rms}$ [A]**
1000 @ 248.25	MS1	7.27	0.96	1.10
	MS2	6.24	2.42	1.09
	MS3	7.75	3.94	1.13
800 @ 201.25	MS1	6.09	1.07	0.89
	MS2	5.33	3.05	0.88
	MS3	6.14	6.23	0.88
500 @ 127.25	MS1	4.21	1.78	0.56
	MS2	3.86	4.97	0.56
	MS3	4.04	12.9	0.58
200 @ 50.00	MS1	2.29	3.64	0.22
	MS2	2.29	13.1	0.21
	MS3	2.45	30.8	0.28

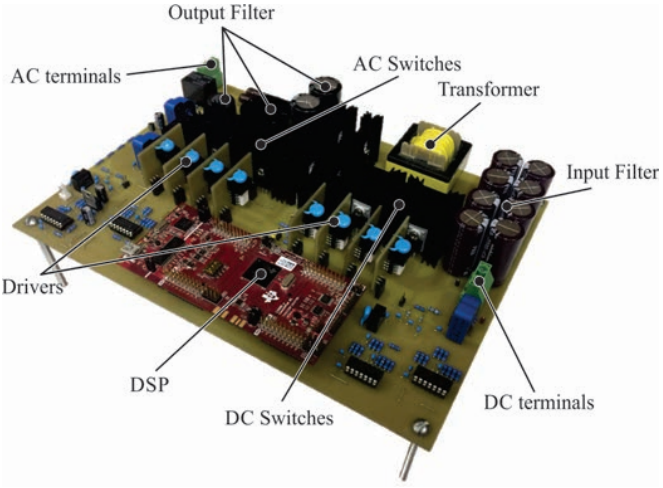

Fig. 4. Prototype of the proposed micro-inverter.

entire grid period as long as power conditions in the load and the source remain unchanged. However, the operation with MS3 since the primary current behavior depends on grid voltage (v_g), so there are minimal and maximum points where it is plausible to exceed the linear operational range of the transformer.

Finally, the experimental efficiency of the prototype for MS1, MS2 and MS3 are compared in Fig. 7. As expected, MS1 features the poorest performance because the two HB to operate at switching frequency and MS3 exhibits the higher efficiency since just input side HF is the only operated at high frequency.

CONCLUSION

Three modulation strategies were compared using the same micro-inverter. The modulation strategy 1 (MS1) demonstrated better harmonic performance at the expense of incurring in low efficiency. The opposite was obtained with modulation strategy 3 (MS3) since it offers the high efficiency in simulation and

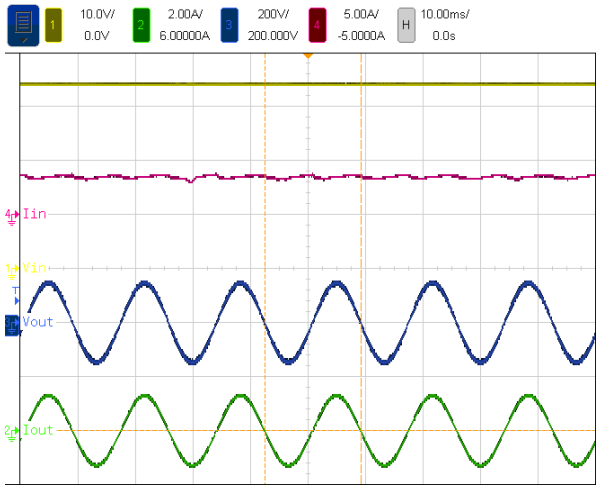

(a)

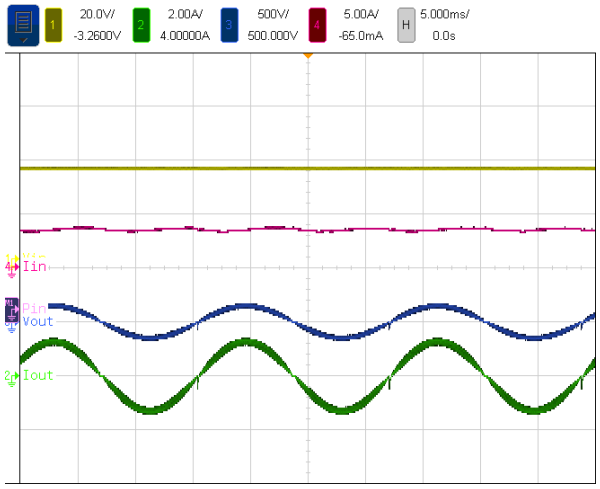

(b)

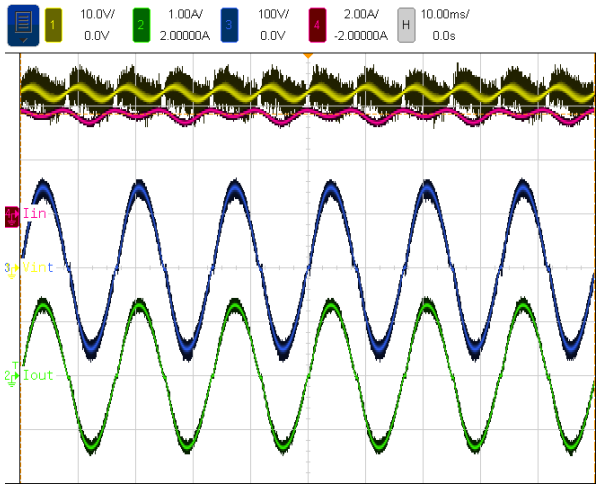

(c)

Fig. 5. Experimental output and input voltages and currents at 120 W for: (a) MS1, (b) MS2, and (c) MS3. CH1: Input voltage V_{in} (yellow), CH2: Output current i_g, CH3: Output voltage v_g and CH4: Output current I_{in}.

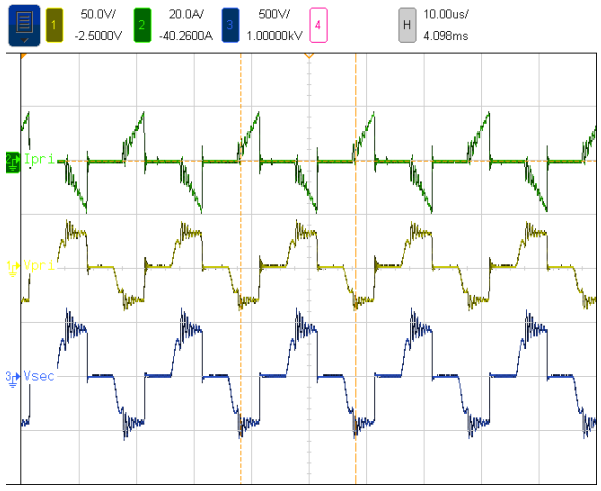

(a)

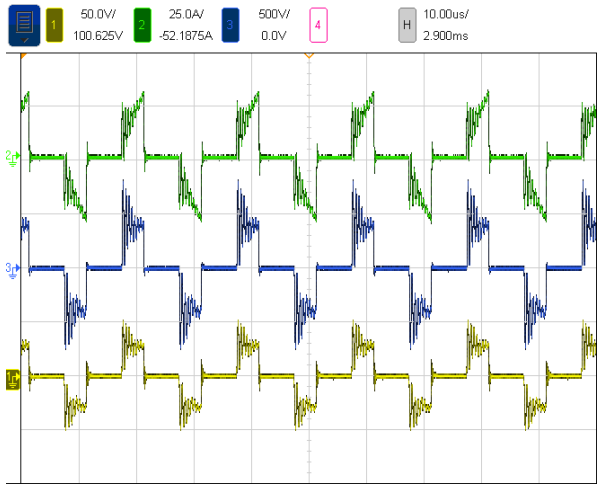

(b)

Fig. 6. Experimental results in the HF transformer obtained from the prototype at 120 W for: (a) MS1 and (b) MS3. CH1: Primary voltage v_{prim} (yellow), CH2: Primary current i_{prim} (green) and CH3: Secondary voltage v_{sec}.

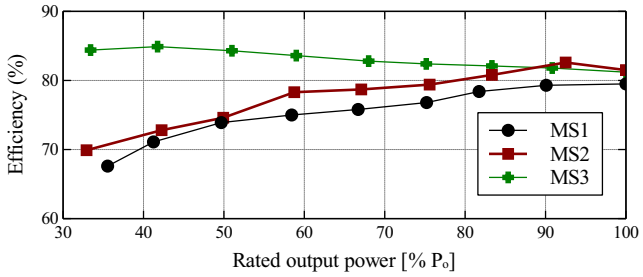

Fig. 7. Experimental efficiency for three modulation strategies.

experimental results and, in return, zero-cross error penalizes the injected grid current THD. Therefore, modulation strategy 2 (MS2) offers an equilibrated performance for both parameters. Experimental results validate the simulation approach.

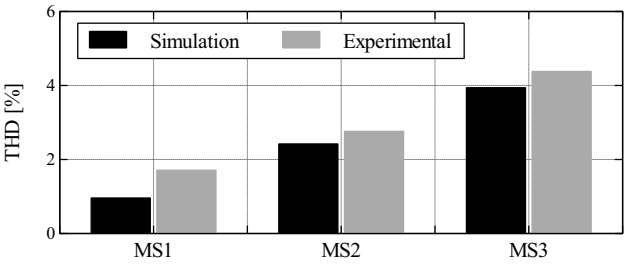

Fig. 8. Comparison of injected current THD at nominal power (120 W).

ACKNOWLEDGMENT

The authors gratefully acknowledge Post–Graduate Program in Electrical Engineering – PPgEE/COPELE, CAPES, CNPq, and FAPESQ for their financial support.

REFERENCES

[1] Renewable Energy Policy Network for the 21st Century (REN21), "Renewables 2017 Global Status Report," Renewable Energy Policy Network for the 21st Century (REN21), Paris, France, Tech. Rep., 2017.

[2] E. Romero-Cadaval, G. Spagnuolo, L. G. Franquelo, C. A. Ramos-Paja, T. Suntio, W. M. Xiao, L. Garcia Franquelo, C. A. Ramos-Paja, T. Suntio, and W. M. Xiao, "Grid-Connected Photovoltaic Generation Plants: Components and Operation," *IEEE Industrial Electronics Magazine*, vol. 7, no. 3, pp. 6–20, 2013.

[3] S. Kouro, J. I. Leon, D. Vinnikov, and L. G. Franquelo, "Grid-connected photovoltaic systems: An overview of recent research and emerging pv converter technology," *IEEE Industrial Electronics Magazine*, vol. 9, no. 1, pp. 47–61, March 2015.

[4] S. B. Kjaer, J. K. Pedersen, and F. Blaabjerg, "A review of single-phase grid-connected inverters for photovoltaic modules," *IEEE Transactions on Industry Applications*, vol. 41, no. 5, pp. 1292–1306, Sept 2005.

[5] R. Carbone and A. Tomaselli, "Recent advances on ac pv-modules for grid-connected photovoltaic plants," in *2011 International Conference on Clean Electrical Power (ICCEP)*, June 2011, pp. 124–129.

[6] Y. Xue, L. Chang, S. B. Kjaer, J. Bordonau, and T. Shimizu, "Topologies of single-phase inverters for small distributed power generators: an overview," *IEEE Transactions on Power Electronics*, vol. 19, no. 5, pp. 1305–1314, Sept 2004.

[7] Q. Li and P. Wolfs, "A review of the single phase photovoltaic module integrated converter topologies with three different dc link configurations," *IEEE Transactions on Power Electronics*, vol. 23, no. 3, pp. 1320–1333, May 2008.

[8] J. S. Lai, "Power conditioning circuit topologies," *IEEE Industrial Electronics Magazine*, vol. 3, no. 2, pp. 24–34, June 2009.

[9] Y. Fang and X. Ma, "A Novel PV Microinverter With Coupled Inductors and Double-Boost Topology," *Power Electronics, IEEE Transactions on*, vol. 25, no. 12, pp. 3139–3147, 2010.

[10] B. Yang, W. Li, Y. Zhao, and X. He, "Design and Analysis of a Grid-Connected Photovoltaic Power System," *Power Electronics, IEEE Transactions on*, vol. 25, no. 4, pp. 992–1000, 2010.

[11] Y. Huang, M. Shen, F. Z. Peng, and J. Wang, "Z-Source Inverter for Residential Photovoltaic Systems," *Power Electronics, IEEE Transactions on*, vol. 21, no. 6, pp. 1776–1782, nov 2006.

[12] Y. Zhou and W. Huang, "Single-Stage Boost Inverter With Coupled Inductor," *Power Electronics, IEEE Transactions on*, vol. 27, no. 4, pp. 1885–1893, 2012.

[13] T. Shimizu, K. Wada, and N. Nakamura, "A flyback-type single phase utility interactive inverter with low-frequency ripple current reduction on the DC input for an AC photovoltaic module system," in *Power Electronics Specialists Conference, 2002. pesc 02. 2002 IEEE 33rd Annual*, vol. 3, 2002, pp. 1483–1488 vol.3.

[14] D. Meneses, O. Garcia, P. Alou, J. A. Oliver, R. Prieto, and J. A. Cobos, "Single-stage grid-connected forward microinverter with constant off-time boundary mode control," in *Applied Power Electronics Conference and Exposition (APEC), 2012 Twenty-Seventh Annual IEEE*, 2012, pp. 568–574.

[15] A. Trubitsyn, B. J. Pierquet, A. K. Hayman, G. E. Gamache, C. R. Sullivan, and D. J. Perreault, "High-efficiency inverter for photovoltaic applications," in *2010 IEEE Energy Conversion Congress and Exposition*, 2010, pp. 2803–2810.

[16] N. Kummari, S. Chakraborty, and S. Chattopadhyay, "An Isolated High-frequency Link Microinverter Operated with Secondary-Side-Modulation for Efficiency Improvement," *IEEE Transactions on Power Electronics*, vol. PP, no. 99, p. 1, 2017.

[17] R. K. Surapaneni, D. B. Yelaverthi, A. K. Rathore, and H. Geng, "Comparative study of cycloconverter based double-ended isolated microinverter topologies for solar photovoltaic AC (SPVAC) module," in *2015 IEEE Industry Applications Society Annual Meeting*, oct 2015, pp. 1–8.

[18] D. Cao, S. Jiang, F. Z. Peng, and Y. Li, "Low cost transformer isolated boost half-bridge micro-inverter for single-phase grid-connected photovoltaic system," in *2012 Twenty-Seventh Annual IEEE Applied Power Electronics Conference and Exposition (APEC)*, feb 2012, pp. 71–78.

[19] S. Jiang, D. Cao, Y. Li, and F. Z. Peng, "Grid-Connected Boost-Half-Bridge Photovoltaic Microinverter System Using Repetitive Current Control and Maximum Power Point Tracking," *Power Electronics, IEEE Transactions on*, vol. 27, no. 11, pp. 4711–4722, nov 2012.

[20] X. Li and A. K. S. Bhat, "A Comparison Study of High-Frequency Isolated DC/AC Converter Employing an Unfolding LCI for Grid-Connected Alternative Energy Applications," *IEEE Transactions on Power Electronics*, vol. 29, no. 8, pp. 3930–3941, aug 2014.

[21] P. Channegowda and V. John, "Filter optimization for grid interactive voltage source inverters," *IEEE Transactions on Industrial Electronics*, vol. 57, no. 12, pp. 4106–4114, Dec 2010.

[22] M. Ciobotaru, R. Teodorescu, and F. Blaabjerg, "A new single-phase PLL structure based on second order generalized integrator," in *2006 37th IEEE Power Electronics Specialists Conference*, jun 2006, pp. 1–6.

[23] ——, "Control of single-stage single-phase PV inverter," in *Power Electronics and Applications, 2005 European Conference on*, sep 2005, pp. 10 pp.–P.10.